

Intermediate-mass stars and the origin of the gas-giant planet-metallicity correlation.

J. Maldonado¹, G. M. Mirouh², I. Mendigutía³, B. Montesinos³, J. L. Gragera-Más^{3,4}, and E. Villaver⁵

¹ INAF - Osservatorio Astronomico di Palermo, Piazza del Parlamento 1, 90134 Palermo, Italy
e-mail: jesus.maldonado@inaf.it

² Instituto de Astrofísica de Andalucía (CSIC), Glorieta de la Astronomía s/n, 18008, Granada, Spain

³ Centro de Astrobiología (CAB) CSIC-INTA, ESA-ESAC Campus, 28692, Villanueva de la Cañada, Madrid, Spain

⁴ Departamento de Física de la Tierra y Astrofísica, Facultad de Ciencias Físicas, Universidad Complutense de Madrid, 28040, Madrid, Spain

⁵ Instituto de Astrofísica de Canarias, 38200 La Laguna, Tenerife, Spain

Received September 15, 1996; accepted March 16, 1997

ABSTRACT

Context. Currently, the number of known planets around intermediate-mass stars ($1.5 M_{\odot} < M_{\star} < 3.5 M_{\odot}$) is rather low and, as a consequence, models of planet formation have their strongest observational evidence on the chemical signature of mostly low-mass (FGK) Main-Sequence (MS) stars with planets.

Aims. We aim to test whether the well-known correlation between the metallicity of the star and the presence of gas-giant planets found for MS low-mass stars still holds for intermediate-mass stars. In particular, we aim to understand whether or not the planet-metallicity relation changes as stars evolve from the pre-MS to the red giant branch.

Methods. We compile the basic stellar parameters (metallicity, mass and age) of a sample of intermediate-mass stars at different evolutionary phases with and without evidence suggesting that they host gas-giant planets. The metallicities of the different subsamples are compared and set in the context of current models of planet formation and stellar evolution.

Results. Our results confirm that pre-MS stars with transitional discs with gaps show lower metallicities than pre-MS with flat discs. We show a tendency of intermediate-mass stars in the MS to follow the gas-giant planet-metallicity correlation, although the differences in metal content between planet and non-planet hosts are rather modest and the strength of the correlation is significantly lower than for the less massive FGK MS stars. For stars in the red giant branch, we find a strong planet-metallicity correlation, compatible with that found for FGK MS stars. We discuss how the evolution of the mass in the convective zone of the star's interior might affect the measured metallicity of the star. In particular, if the planet-metallicity correlation were of primordial origin, one would expect it to be stronger for less massive stars, as they are longer convective during the stellar evolution. However, within our sample, we find the opposite.

Conclusions. The lack of a well-established planet-metallicity correlation in pre-MS and MS intermediate-mass stars can be explained by a scenario in which planet formation leads to an accretion of metal-poor material on the surface of the star. As intermediate-mass stars are mainly radiative the metallicity of the star does not reflect its bulk composition but the composition of the accreted material. When the star leaves the MS and develops a sizeable convective envelope, a strong-planet metallicity correlation is recovered. Thus, our results are in line with core-accretion models of planet formation and the idea that the planet-metallicity correlation reflects a bulk property of the star.

Key words. techniques: spectroscopic — stars: abundances — stars: early-type — planetary systems

1. Introduction

Understanding the origin of stars and planetary systems is one of the major goals of modern astrophysics. Almost thirty years of exoplanetary science has unveiled an astonishing diversity of planetary architectures as well as host stars. Exoplanets have been discovered not only around solar-like Main-Sequence (MS) stars but also around brown dwarfs and low-mass stars, metal-poor stars, giant stars as well as white dwarfs and pulsars (e.g. Perryman 2018). However, the bulk majority of known exoplanets is still found to orbit around MS stars. In turn, only about 5% of known exoplanets are found around stars with masses between 1.5 and $3.5 M_{\odot}$, based on the available data at The Extrasolar Planets Encyclopaedia¹ (Schneider et al. 2011).

The role of the host star's chemical composition in planet formation has been largely discussed, with the finding that the frequency of gas-giant planets is a strong function of the stellar metallicity (e.g. Gonzalez 1997; Santos et al. 2004; Fischer & Valenti 2005). Observations of solar-type, FGK dwarfs, MS planet hosts point towards a metal rich nature of the MS stars Fischer & Valenti (2005) showed that the probability of formation of a gas-giant planet around an FGK-type dwarf depends on the square of the number of iron atoms, in agreement with the expectation from the collisional agglomeration of dust grains. Other explanations invoking the late-stage accretion of metal-depleted material onto the convective zone of the star (Gonzalez 1997; Laughlin & Adams 1997) were ruled out.

Intermediate-mass stars from pre-MS and MS to giants offer the unique opportunity of testing how well founded the planet-metallicity relation is, how it changes as the star evolves, and

¹ <https://exoplanet.eu/home/>

to unravel its origin. At the time of writing, no planets have been confirmed around young, intermediate-mass Herbig stars (Brittain et al. 2023), although several candidates have been proposed. For example, an accreting protoplanet has been proposed in the disc around the Herbig star AB Aurigae (Currie et al. 2022) but its detection is the subject of debate (Biddle et al. 2024). Nevertheless, high-resolution imaging surveys have shown that many Herbig stars show cavities in their discs, potentially carved out by giant planets (e.g. Garufi et al. 2017; Stapper et al. 2022a,b). Based on their spectral energy distributions, the discs around Herbig stars are usually classified as warm, flaring, group I and cold, flat, group II (Meeus et al. 2001). Group I sources have transitional discs with radial cavities or gaps. Kama et al. (2015) proposed that flaring group I sources show a deficit of refractory elements, and thus low values of metallicity. Recently, Guzmán-Díaz et al. (2023) confirmed that group I sources tend to have a lower metallicity than group II sources, as well as that group I sources tend to have stronger (sub-) mm continuum emission likely related to the presence of giant planets. This suggests that giant planets should be frequent around group I/low metallicity Herbig stars. According to Kama et al. (2015) and Jermyn & Kama (2018), forming planets in group I sources trap the metal-rich material, while metal-depleted material continues to flow towards the central star.

Herbig stars will eventually evolve into early-type MS stars (e.g. Brittain et al. 2023). Early-type stars are not optimal targets for radial velocity and transit measurements. Their spectra show few spectral lines that, in addition, are quite broad and shallow due to the high projected rotation of the star. Therefore, it is difficult to determine the centroid position of the lines and thus a Doppler shift. On the other hand, transit detections are challenged by the expected small transit depths and long transit duration. As a result the number of known exoplanets around intermediate-mass ($M_{\star} > 1.5 M_{\odot}$) MS is rather low if compared with the number of planets known around their less massive counterparts. Previous analysis of the chemical patterns of early-type stars with planets has focused in the study of a likely relation between peculiar chemical patterns like those of λ Boötis and metallic-lined A stars, with the presence of giant planets (Saffe et al. 2021, 2022), finding that there is no a unique chemical pattern for these stars.

The post-MS red giant stars that we observe today are the result of the evolution of early-type MS dwarfs. Whether the correlation between gas-giant planet occurrence and metallicity extends to giant stars has been the subject of an intense debate, as several studies have found contradictory results (see e.g. Maldonado et al. 2013, and references therein). In order to explain the apparent lack of a clear planet-metallicity correlation in giant stars several interpretations have been put forward. These invoke scenarios like the accretion of metal-rich material, higher-mass protoplanetary discs or the formation of massive gas-giant planets by gravitational instabilities. In addition, the architecture of planetary systems around evolved stars show some peculiarities with respect to the planets orbiting around MS stars, such as a lack of close-in planets or higher masses and eccentricities (e.g. Maldonado et al. 2013).

In this work, we aim to unravel the gas-giant planet - stellar metallicity relationship for intermediate mass stars ($1.5 M_{\odot} < M_{\star} < 3.5 M_{\odot}$) through the formation of stars and planets until the last stages of their evolution. The paper is organised as follows: Sect. 2 describes the stellar samples analysed in this work and how stellar parameters are obtained. The metallicity distributions are presented in Sect. 3. The results are discussed at length in Sect. 4. Our conclusions follow in Sect. 5.

2. Stellar sample

Our stellar sample is composed of a total of 131 of stars at different evolutionary stages, namely the pre-MS phase, the MS, and the red giant phase. The subsample of intermediate-mass, pre-MS stars was taken from Guzmán-Díaz et al. (2023). It is composed by 67 Herbig stars with spectral types later than B8 (i.e., T_{eff} below 12000 K). We discarded those stars without a group I/II SED classification (five stars) as well as the stars with only a lower or upper limit in their metallicities' estimates (11 stars). We performed an additional cut and discarded the group II targets more massive than $\sim 3.5 M_{\odot}$ (six stars). This cut is needed, as no group I star has a mass larger than $3.0 M_{\odot}$, whilst the discarded group II stars might have masses as large as $\sim 7.0 M_{\odot}$. The selected pre-MS stars cover a range of ages between 2 and 20 Myr, and it is composed of 20 group I sources and 24 group II sources. Stellar parameters and group I/II classification were derived from a combination of spectra and photometry (Guzmán-Díaz et al. 2021). Through this paper we will make the assumption that the gap inferred in the protoplanetary disc of group I stars is due to the presence of (at least) one giant-planet (Guzmán-Díaz et al. 2023). In the same line, group II stars will form the corresponding comparison sample, that is, the sample of pre-MS stars without known planets.

The subsample of MS intermediate-mass stars with and without known planets is drawn from Saffe et al. (2021, 2022). It is composed by a total of 28 stars (13 planet hosts; 15 stars without known gas-giant companions). The stellar mass varies between 1.5 and $2.2 M_{\odot}$, whilst the stars have ages ranging from 144 Myr to 1.5 Gyr. Stellar parameters are determined in a homogeneous way from high-resolution spectra (Saffe et al. 2021, 2022).

The subsample of post-MS, giant stars mainly comes from Maldonado et al. (2013) and Maldonado & Villaver (2016) to which we added six additional planet-hosts not previously analysed. The selected giant sample covers a range of stellar masses between 1.5 and $3.6 M_{\odot}$ and ages between 240 Myr and 3 Gyr. It is composed of 21 planet hosts and 38 comparison stars (that is, stars without known companions). Stellar parameters were derived from high resolution spectroscopy and photometry (Maldonado et al. 2013).

Figure 1 shows the Hertzsprung-Russell (HR) diagram of the stars studied in this work, whilst the main properties of the sample are provided in Appendix A. Given that the planet-metallicity correlation applies only to gas-giant planets (e.g. Ghezzi et al. 2010; Sousa et al. 2011), before we proceed with the analysis, we carefully checked that all the planets in the MS and giant star subsamples have (minimum)-masses larger than $30 M_{\oplus}$, which is also the type of planets that should be expected around group I pre-MS stars.

3. Analysis

The cumulative distribution function of the metallicity for the different subsamples analysed in this work is presented in Fig. 2. For guidance some statistical diagnostics are also provided in Table 1. To assess whether the metallicity distribution of both comparison and planet-hosts are equal from a statistical point of view, for each subsample, we performed two different statistical tests: a standard two-sample Kolmogorov-Smirnov (K-S) (e.g. Peacock 1983) and the Anderson-Darling (A-D) (e.g. Scholz & Stephens 1987) test.

There are a few interesting facts to be derived from these distributions and their statistical tests. Group I pre-MS stars tend to have a lower metallicity distribution than group II pre-MS

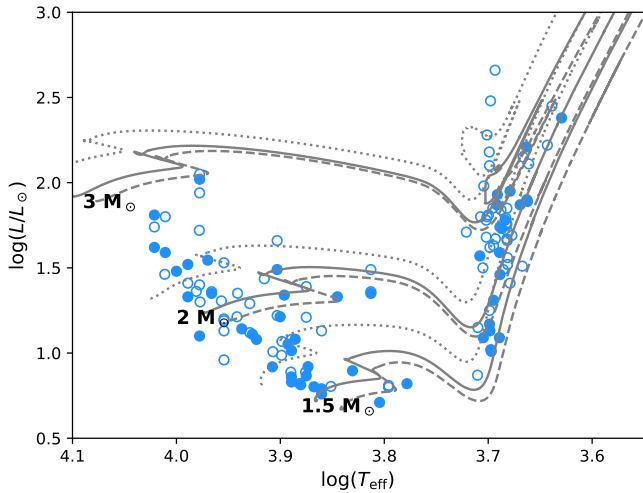


Fig. 1. Luminosity versus T_{eff} diagram for the observed stars. Planet hosts are plotted with filled symbols. Evolutionary tracks computed with MESA are overplotted (see text). For each mass, three tracks are plotted, corresponding to $[\text{Fe}/\text{H}] = -0.40$ ($Z = 0.0057$, dotted lines), $[\text{Fe}/\text{H}] = +0.00$ ($Z = 0.0142$, solid lines), and $[\text{Fe}/\text{H}] = +0.20$ ($Z = 0.0225$, dashed lines).

stars. The K-S test confirms that both distributions differ within a confidence level of 99.9%, in agreement with the A-D test that shows that the null hypothesis that the comparison and the planet host metallicity distribution are similar (come from the same parent population) can be rejected at the 0.1% level as the returned test value (6.76) is greater than the critical value for 0.1% (6.55). If we take the assumption that the disc structures found on group I sources are likely related to the presence of gas-giant planets, that means that pre-MS planet-hosts do not show metal enrichment, but rather a deficit of metals with respect to their respective comparison sample. This result confirms the previous findings of Kama et al. (2015) and Guzmán-Díaz et al. (2023).

For intermediate-mass MS stars there seems to be a tendency of planet hosts to have slightly larger metallicity values than their corresponding comparison sample. However, none of the performed statistical tests confirms this fact. The K-S test provides a probability that both samples (planet hosts and comparison stars) share a similar metallicity distribution of roughly 60%, whilst from the A-D we just simply cannot reject the null hypothesis that the comparison and the planet host metallicity distribution are similar.

We find that the gas-giant planet - stellar metallicity correlation is also present in intermediate-mass giant stars in agreement with recent works (e.g. Maldonado et al. 2013; Reffert et al. 2015; Wolthoff et al. 2022). The A-D test shows that the metallicity distribution of planet hosts and comparison stars differ at the 5% level although not at the 2.5% level.

Figure 3 shows the frequency of gas-giant planets as a function of the stellar metallicity for the different subsamples. That is, for each metallicity bin, the number of known gas-giant planets is divided by the total number of stars of the bin. The uncertainties in the frequency of each bin are calculated using the binomial distribution (each star either has or not has a planet),

$$P(f_p, n, N) = \frac{N!}{n!(N-n)!} f_p^n (1-f_p)^{N-n} \quad (1)$$

where $P(f_p, n, N)$ provides the probability of n detections given a sample of size N when the true planetary companion frequency is f_p . We follow the common practice of reporting the range in planetary fraction that delimits 68.2% of the integrated probability function, which is equivalent to the 1σ limits for a Gaussian distribution (see e.g. Burgasser et al. 2003; Endl et al. 2006).

Following previous works (Fischer & Valenti 2005; Udry & Santos 2007), the fraction of stars with planets was fitted to a function with a function of the form,

$$f([\text{Fe}/\text{H}]) = C \times 10^{\alpha[\text{Fe}/\text{H}]} \quad (2)$$

The derived α values are provided in Table 1. For pre-MS stars, we see that the distribution peaks at metallicities around -0.25 , and then, for higher metallicity values, it remains flat. As a consequence, the derived α value is slightly negative ~ -0.29 . MS and giant stars show the well-known planet metallicity correlation, although with some differences. For intermediate-mass MS the strength of the correlation, α is only ~ 0.5 which is significantly lower than the value found for their less massive FGK MS counterparts, $\alpha \sim 2$ (Fischer & Valenti 2005). On the other hand, for giants, we found a strong planet-metallicity correlation with a parameter $\alpha \sim 1.6$ which is compatible with the correlation found for FGK-type MS stars.

In order to further test the planetary frequency as a function of the stellar metallicity, we use a Bayesian approach. Details of the analysis can be found in e.g. Johnson et al. (2010); Maldonado et al. (2020). In brief, the planetary frequency is related to metallicity through Eq. 2, with $X = (C, \alpha)$ being the parameters to be optimised. We model the data as a series of Bernoulli trials. The probability of a specific model X , considering our data d is given by the Bayes theorem:

$$P(X|d) \propto P(X) \prod_i^H f([\text{Fe}/\text{H}]_i) \times \prod_j^{T-H} [1 - f([\text{Fe}/\text{H}]_j)] \quad (3)$$

where T is the total number of stars and H is the number of planet hosts. The likelihood is then given by:

$$\mathcal{L} \equiv \log P(X|d) \propto \sum_i^H \log f([\text{Fe}/\text{H}]_i) + \sum_j^{T-H} \log [1 - f([\text{Fe}/\text{H}]_j)] + \log P(X) \quad (4)$$

In order to account for uncertainties in the metallicity determination, we assume a Gaussian probability distribution with mean ($[\text{Fe}/\text{H}]_i$) and standard deviation ($\sigma_{[\text{Fe}/\text{H}]_i}$). In this way, the predicted planet fraction for the i th star is:

$$f([\text{Fe}/\text{H}]_i) = \int p_{\text{obs}}([\text{Fe}/\text{H}]_i) f([\text{Fe}/\text{H}]) d[\text{Fe}/\text{H}] \quad (5)$$

Our results are shown in Table 1 where the mean α values and their corresponding uncertainties are provided, while Fig. A.1 shows the marginal posterior probability. The Bayesian analysis confirms the results from the bin fitting. That is, intermediate-mass MS planet hosts show a weaker planet-metallicity correlation than giant stars, while pre-MS stars show an anti-correlation.

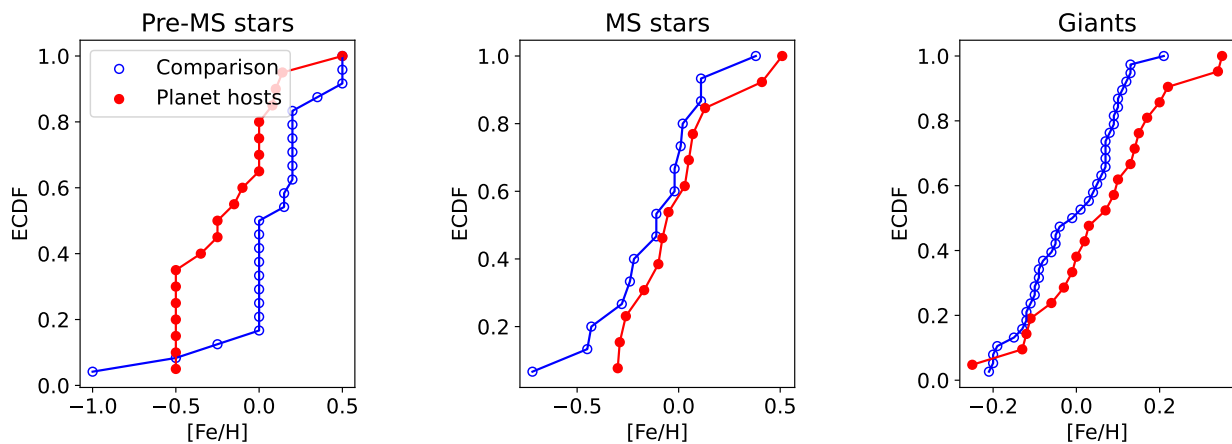


Fig. 2. Comparison of the $[\text{Fe}/\text{H}]$ empirical cumulative distribution function (ECDF) between planet hosts (red circles) and stars without known planets (blue circles) for the different subsamples studied in this work, from pre-MS stars to giants.

Table 1. Comparison between the $[\text{Fe}/\text{H}]$ of the different subsamples. For each subsample we list the number of stars (N) as well as the mean and the standard deviation values of the $[\text{Fe}/\text{H}]$ distribution. For the statistical tests, we provide the test statistic value, D , as well as the asymptotic p -value. The A-D test critical values for significance levels of 5%, 2.5%, 1%, 0.5%, and 0.1% are 1.96, 2.72, 3.75, 4.59, and 6.55, respectively. Values of α , defined as in Eq. 2, are provided for the bin fitting as well as for the Bayesian fit.

Sample	Comparison			Planet hosts			K-S test		A-D test		α	
	N	Mean	σ	N	Mean	σ	D	p -value	D	p -value	Bin fitting	Bayesian fit
pre-MS	24	0.07	0.31	20	-0.20	0.28	0.47	0.001	6.76	0.002	-0.29 ± 0.13	-1.40 ± 0.83
MS	15	-0.11	0.26	13	-0.05	0.25	0.26	0.610	-0.21	0.456	0.50 ± 0.19	0.80 ± 0.60
Giants	38	0.00	0.11	21	0.07	0.15	0.31	0.121	2.31	0.040	1.64 ± 0.42	1.77 ± 0.85

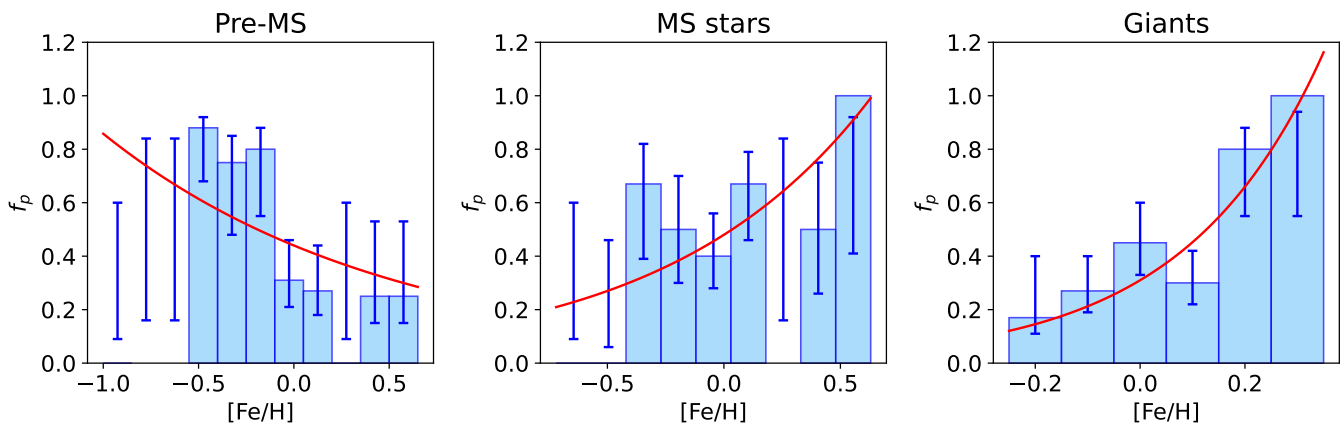


Fig. 3. Frequency of gas-giant planets as a function of the stellar $[\text{Fe}/\text{H}]$ for each of the subsamples analysed in this work. The best bin fitting is shown in red. Vertical lines show the range in planetary fraction that delimits 68.2% of the integrated probability function (see Eq. 1).

4. Discussion

In this section we discuss our results in the framework of current planet formation models. The two main formation models for giant planets are the core accretion and the disc instability. The core accretion model starts with the formation of a massive planet core, followed by a rapid accumulation of a massive gas envelope. Within this framework, a high metallicity environment implies a high dust-to-gas-ratio in the protoplanetary disc that facilitates condensation, and accelerates accretion before the gas disc is lost (e.g. Pollack et al. 1996; Rice & Armitage 2003; Alibert et al. 2004; Mordasini et al. 2012). In the gravitational disc instability, giant planets form by the contraction of gaseous condensations in a massive self-gravitating disc (e.g. Boss 2002, 2017). Although initial disc instability models are not able to ex-

plain the correlation of giant planet occurrence and stellar metallicity, the inclusion of pebble accretion into the models might overcome this difficulty (Nayakshin 2015).

4.1. Core accretion

As pointed out in Sect. 3 we find that the metallicity distribution of pre-MS Herbig group I stars is shifted towards lower values with respect to the one of its corresponding group II comparison sample, in agreement with previous claims (Guzmán-Díaz et al. 2023). Assuming that the cavities found in group I sources are carved out by the presence of gas-giant planets, this seems to imply that pre-MS stars with planets do not follow the gas-giant planet-metallicity correlation. Indeed, our analysis points out that the frequency of gas-giant planets around pre-

MS star does not depend on the stellar metallicity or even might show an anticorrelation. Although this result apparently contradicts the gas giant planet-metallicity correlation, it may be explained within the theoretical framework by Kama et al. (2015) and Jermyn & Kama (2018). According to these authors, forming planets in protoplanetary discs block the accretion of part of the dust, while gas continues to flow towards the star. Given that Herbig stars have radiative envelopes, the mixing timescales with the interior are large, of the order of several Myr. Thus, metallicity measurements reflect the metal composition of the accreted metal-poor material that pollutes the external layers of the star. Numerical simulations of the evolution of pre-MS stars have shown that stars with $T_{\text{eff}} > 7000$ K may show large metallicity deficits, by 0.6 dex or more, in the presence of efficient planet formation (Kunitomo et al. 2018).

Herbig stars evolve into early-type MS stars within a characteristic time scale of a few Myr. Typical timescales are of the order of ~ 3 Myr for a $3 M_{\odot}$ star and ~ 20 Myr for a $1.5 M_{\odot}$ star. Therefore, slow non-convective processes (see e.g. Jermyn & Kama 2018) might have partially mixed the metal-poor accreted material during the pre-MS phase with the interior. Thus, under the assumption that gas-giant planets form in metal-rich environments, the question is whether or not the non-convective processes in intermediate mass MS stars are able to reset the original metal-rich composition of the star. Our results suggest a rather weak planet metallicity correlation with $\alpha \sim 0.8$. This implies that, if the planet-metallicity correlation had a primordial origin, then, the slow mixing processes in stars with a radiative surface are able to partially recover the bulk composition of the star. However, we should caution that this interpretation needs of a robust statistical confirmation. As we have seen in Sect. 3, we cannot rule out the possibility that planet hosts show a similar metallicity distribution that stars without known planets.

In the hypothesis that the observed correlation between the metallicity of the star and the presence of gas-giant hosts is a bulk property of the star, it should also hold for red giants that are convective for the most part. As shown before, we found a strong planet-metallicity correlation for red giants that is compatible with the correlation found for low-mass FGK MS stars. Thus, our results support the idea that gas-giant planets are more easily formed in high metallicity environments.

4.2. Planet-metallicity correlation and the role of convective envelopes.

In order to unravel the possible role of the convective zone in the gas-giant planet-metallicity correlation, we compute a series of evolutionary tracks by using the Modules for Experiments in Stellar Astrophysics (MESA) package (Paxton et al. 2011, 2013, 2015, 2018, 2019; Jermyn et al. 2023). Tracks were computed for stellar masses between $1.5 M_{\odot}$ and $3.5 M_{\odot}$ by using the solar composition ($Y=0.2703$, $Z=0.0142$) from Asplund et al. (2009) and a mixing length parameter of 1.82. The simulations do not include overshooting, semi-convection or mass-loss processes. Figure 4 shows the evolution of the thickness and mass included in the convection zone of intermediate-mass stars.

Newly born, pre-MS stars are fully convective. However, they develop a radiative envelope in a short timescale. This timescale is mass-dependent and more massive stars (blue line) turn on radiative more rapidly.

For MS stars, it can be seen that irrespective of their masses, they remain with a radiative envelope during their MS evolution. While a tendency towards slightly larger convective zones dur-

ing their evolution can be seen, the mass in the convective zone remains always below $\sim 10^{-5}$ the total mass of the star.

Finally, stars at the beginning of the Hertzsprung gap and the red giant phase have a radiative envelope. They develop a convective zone during their evolution across the Hertzsprung gap/subgiant phase. The models show that less-massive stars (red line) develop a convective envelope more rapidly than the more-massive stars (blue line).

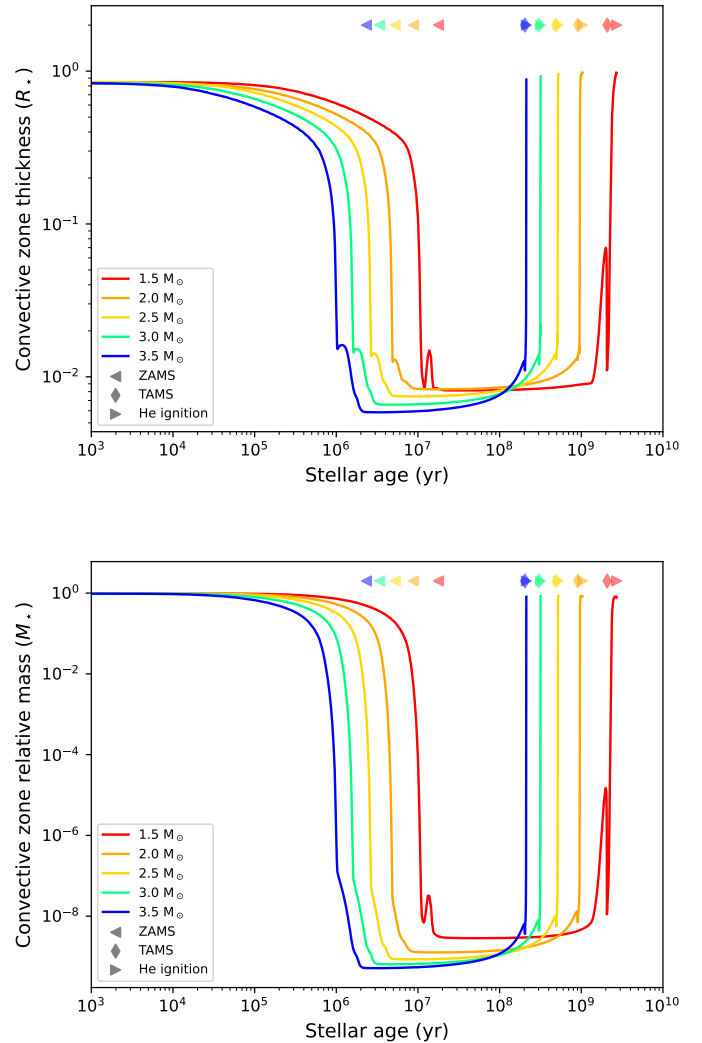


Fig. 4. Top panel: thickness of the surface convection zone, bottom panel: mass included in said convection zone (zero means no surface convection and one means an entirely convective star). The symbols mark the zero-age main-sequence (leftward triangle), the terminal-age main sequence (diamond) and helium ignition (rightward triangle). Different colours indicate different stellar masses.

These results imply that stellar evolution plays a fundamental role in our understanding of the gas-giant planet-metallicity correlation. In summary, models predict that high-mass stars with planets should be longer radiative, both in the pre-MS as well as in the red giant phase, and therefore are likely to be more polluted by the accretion of metal-poor material than low-mass stars. In other words, the stellar surfaces of lower mass stars should better reflect primordial compositions because mixing by convection lasts longer for these stars. Therefore, if we assume that the observed planet-metallicity correlation has a pri-

mordial origin, we might expect it to be stronger for the less massive stars. In order to test whether this effect is or not present in our sample, we divide the different samples into “less massive” and “more massive” by imposing a mass cut-off. In order to avoid using a somehow arbitrary cut-off and/or small subsamples size, five different values of mass were considered for the cut. The parameter α (defined in Eq. 2) was taken as a measure of the “strength” of the planet-metallicity correlation and a Bayesian analysis was performed for each subsample. The results are shown in Fig. 5 where the derived α values are shown for the less-massive (green symbols) and more-massive (blue colour) subsamples as a function of the mass value used for the cut-off.

For pre-MS stars we obtain a somehow stronger planet-metallicity correlation for the more massive stars, in disagreement with our expectations. We note that the derived α values are not dependent on the mass used to define the high- and low-mass subsamples. On the other hand, when considering the stars in the MS and in the red giant phase, we also find that the planet-metallicity correlation is clearly stronger for the more-massive stars that remain radiative longer than their less-massive counterparts. Again, this result contradicts our expectation. Furthermore, we find a strong dependency of α on the selected cut-off mass, which can take values as high as six when considering a mass cut-off $\geq 2.0 M_{\odot}$.

4.3. Caveats and possible scenarios

The previous contradictory results lead us to the question of whether or not some biases might affect our results. To start with, we note that the sample sizes are reduced significantly when applying the mass cut-off. Second, even if the formal errors in the stellar masses are rather low, the accurate determination of stellar masses for pre-MS and giants stars is rather difficult as the evolutionary tracks are very close and small changes in temperature, luminosity or stellar metallicity might be of importance. Furthermore, it could be the case that the difference in mass between the less- and more- massive stars is not large enough to find a statistically significant difference. For example, if we set the mass cut-off at $2.1 M_{\odot}$ then, the mean mass of the less-massive pre-MS is $1.8 M_{\odot}$ while the mean mass of the more-massive pre-MS is $2.5 M_{\odot}$ (similarly, for giants we have mean masses of $1.7 M_{\odot}$ and $2.6 M_{\odot}$ for the less- and more- massive stars, respectively). Furthermore, we caution that the uncertainties in the derived α values are rather large.

In addition, planet engulfment can produce refractory element enhancements within the engulfing star convective region due to ingestion of rocky planetary material (e.g. Oh et al. 2018). In a recent work, Mendigutía et al. (2024) shows that stellar magnetospheres act as a protoplanetary disc barrier preventing unlimited planet migration. As discussed in that work, magnetospheres become smaller as the stellar mass increases, potentially disappearing in Herbig stars with masses $\geq 3-4 M_{\odot}$ (Wichittanakom et al. 2020; Vioque et al. 2022). Thus, planet engulfment by intermediate-mass host stars is more likely as the stellar mass increases, which is in line with the mass dependence of the planet metallicity correlation we found for the pre-MS and MS samples. Along this line, Soares et al. (2025) show that engulfed planets have a higher amount of refractories and that engulfment is more likely to occur in systems that come from more massive and more metal-rich protoplanetary discs.

On the other hand, tidal interactions in the star system as the star evolves off the MS can lead to variations in the planetary orbits as well as to the engulfment of close-in planets (Villaver

& Livio 2009). The planet accretion process might lead to a transfer of angular momentum to the stellar envelope, which ultimately can spin up the star and even modify its chemical abundances. This would be in line with the enhancement of the planet-metallicity correlation we find during the post-MS phase.

As we have discussed, more massive stars retain longer their radiative envelopes. Hence, contamination by planet engulfment is expected to be more important. Therefore, the question on whether or not planet engulfment may affect the metallicity content of more massive stars arises. An enrichment in refractory elements produced by planet engulfment may be a suitable explanation for the strong planet metallicity correlation found for the more massive stars, especially for the stars in the red giant phase. However, Villaver et al. (2014) find that planet engulfment along the red giant branch is not very sensitive to the stellar mass or mass-loss rates, but quite sensitive to the planetary mass.

Finally, it should be noted that it is well known that the planet occurrence rate, in addition to the metal content of the star, does also rise monotonically with the stellar mass (e.g. Johnson et al. 2010). However, for all the samples studied here (pre-MS, MS, and red giants) we find a rather flat distribution without any clear mass-planet dependency.

4.4. Can we discard disc instability?

Another possibility is that intermediate-mass stars represent a different stellar population in which a metal-rich environment is not required for planet formation. This would naturally explain the lack of a statistically well-founded giant-planet metallicity correlation in intermediate-mass pre-MS and MS stars. However, we find that giant stars do show the planet-metallicity correlation.

Thus, it is likely that both formation mechanisms, core-accretion and disc instability might simultaneously operate in intermediate-mass stars. The disc mass scales with the stellar mass over several orders of magnitude (see Mendigutía et al. 2012; Manara et al. 2023, and references therein). Detailed simulations have confirmed that massive ($> 0.1 M_{\odot}$) protoplanetary discs might cool rapidly enough to become gravitationally unstable. On the other hand, fragmentation appears less likely to produce giant planets around solar-type FGK stars, where the gas cools too slowly for it to fragment into bound clumps (see Perryman 2018, and references therein).

A disc-to-star mass ratio of 0.1 is the usual threshold for triggering gravitational instability (Kratter & Lodato 2016). However, disc masses inferred from (sub-)mm continuum emission lead to disc-to-star ratios that tend to be an order of magnitude smaller both for low- and intermediate-mass stars (Mendigutía et al. 2012; Guzmán-Díaz et al. 2021; Stapper et al. 2022a). Recently, Mendigutía et al. (2024) argued that gravitational instability is not consistent with the presence of hot Jupiters around intermediate-mass stars, which could be explained via a combination of the core-accretion paradigm and migration. On the other hand, assuming that disc masses are larger than inferred from (sub-)mm continuum emission, Dong et al. (2018) proposed that gravitational instability may explain the multi-arm features commonly observed in discs around Herbig stars. Recently, Speedie et al. (2024) inferred a disc-to-star ratio ~ 0.3 for the protoplanet-candidate host AB Aurigae, also providing kinematic evidence of gravitational instability in its disc.

If gravitational instability were the main mechanism for giant-planet formation in intermediate-mass stars, one would expect a weaker planet-metallicity correlation as the stellar mass increases. This is in disagreement with what we found. Thus,

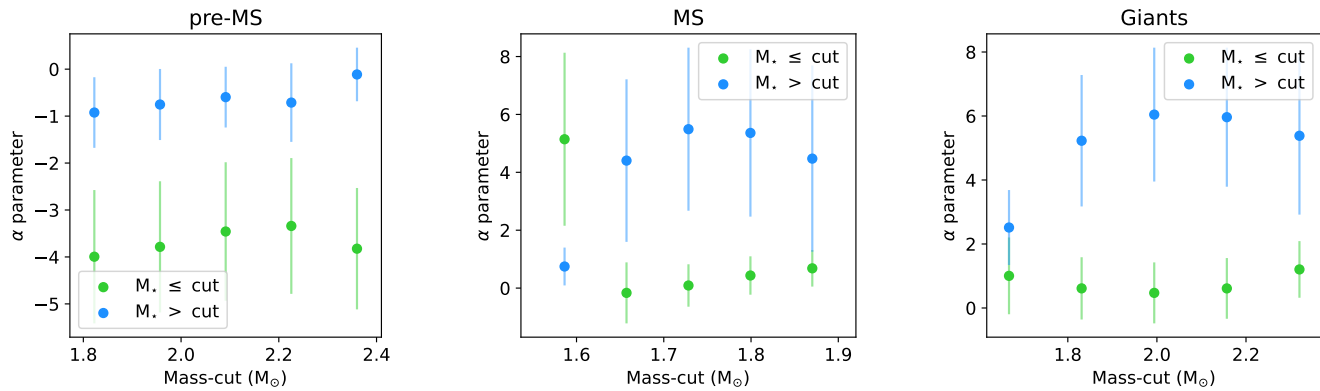


Fig. 5. α values derived for the “less massive” (green) and “more massive” (blue) subsamples as a function of the adopted mass cut-off.

even though some specific planet might still be formed by gravitational instability, our analysis suggests that core-accretion is likely the main formation scenario for gas-giant planets.

5. Conclusions

In this work the metallicity distribution of a large sample of intermediate-mass stars ($1.5 M_{\odot} < M_{\star} < 3.5 M_{\odot}$) at different evolutionary stages is presented with the aim to test the planet-metallicity correlation. We compare the metallicity distribution of stars with and without known gas-giant companions and perform a detailed statistical analysis to quantify the strength of the correlations.

Under the assumption that the gap inferred in the protoplanetary disc of group I stars is related to the formation of giant-planets, we show that intermediate-mass pre-MS do not follow the well known gas-giant planet-metallicity correlation. For MS intermediate-mass stars, a tendency of higher metallicity in planet hosts with respect to its comparison sample is found, but it lacks of statistical support and the strength of the correlation is significantly lower than for FGK MS stars. Intermediate-mass stars in the red giant branch follow a strong-planet metallicity correlation.

By taking into account the internal evolution of the host stars, we show that the previous results are generally more compatible with the core-accretion, scenario of planet formation than with the disc instability scenario. Intermediate-mass pre-MS stars are born fully convective, but they develop a radiative envelope in short-time timescales. Forming planets in group I sources trap the metal-rich material, and since these stars have radiative envelopes, metallicity reflects the composition of the stellar surface, polluted by the accreted metal-poor material. Pre-MS Herbig stars evolve into early-type MS stars which remain radiative during their MS evolution. Slow non-convective processes might partially mix the metal-poor accreted material, thus preventing us from finding a statistically significant planet-metallicity correlation. When early-type stars leave the MS and evolve along the red giant branch they become convective for the most part and the gas-giant planet-metallicity correlation is recovered.

Evolutionary models predict that massive pre-MS stars turn on radiative more rapidly. In addition, massive giants remain longer radiative during their evolution. Therefore, more massive stars should be more affected by the accretion of metal-poor material. However, within our sample, we find that the more massive stars show a stronger planet-metallicity correlation than the less massive stars. We discuss several possible explanations. In particular, we argue that the planet engulfment scenario may

play a role in explaining the previous result, but it deserves a more careful analysis.

A better understanding of the planet-metallicity correlation in intermediate-massive stars will require the detection of larger samples of known planets as well as accurate masses and radii of the host stars. The forthcoming mission PLATO (Rauer et al. 2014) is expected to make systematic use of asteroseismology to characterise planet host stars allowing us to link planetary and stellar evolution. Science targets for PLATO will include massive stars, red giants, asymptotic giant branch stars and supergiants, as well as white dwarfs. These, together with detailed models of diffusion, rotation, and other stellar mixing mechanisms that control how the accreted material onto the stellar surface interchanges with the interior of the star, will help us to unravel the link between stellar abundance patterns and planet formation.

References

- Alibert, Y., Mordasini, C., & Benz, W. 2004, *A&A*, 417, L25
 Asplund, M., Grevesse, N., Sauval, A. J., & Scott, P. 2009, *ARA&A*, 47, 481
 Biddle, L. I., Bowler, B. P., Zhou, Y., Franson, K., & Zhang, Z. 2024, *AJ*, 167, 172
 Boss, A. P. 2002, *ApJ*, 567, L149
 Boss, A. P. 2017, *ApJ*, 836, 53
 Brittain, S. D., Kamp, I., Meeus, G., Oudmaijer, R. D., & Waters, L. B. F. M. 2023, *Space Sci. Rev.*, 219, 7
 Burgasser, A. J., Kirkpatrick, J. D., Reid, I. N., et al. 2003, *ApJ*, 586, 512
 Currie, T., Lawson, K., Schneider, G., et al. 2022, *Nature Astronomy*, 6, 751
 Dong, R., Najita, J. R., & Brittain, S. 2018, *ApJ*, 862, 103
 Endl, M., Cochran, W. D., Kürster, M., et al. 2006, *ApJ*, 649, 436
 Fischer, D. A. & Valenti, J. 2005, *ApJ*, 622, 1102
 Garufi, A., Meeus, G., Benisty, M., et al. 2017, *A&A*, 603, A21
 Ghezzi, L., Cunha, K., Smith, V. V., et al. 2010, *ApJ*, 720, 1290
 Gonzalez, G. 1997, *MNRAS*, 285, 403
 Guzmán-Díaz, J., Mendigutía, I., Montesinos, B., et al. 2021, *A&A*, 650, A182
 Guzmán-Díaz, J., Montesinos, B., Mendigutía, I., et al. 2023, *A&A*, 671, A140
 Jermyn, A. S., Bauer, E. B., Schwab, J., et al. 2023, *ApJS*, 265, 15
 Jermyn, A. S. & Kama, M. 2018, *MNRAS*, 476, 4418
 Johnson, J. A., Aller, K. M., Howard, A. W., & Crepp, J. R. 2010, *PASP*, 122, 905
 Kama, M., Folsom, C. P., & Pinilla, P. 2015, *A&A*, 582, L10
 Kratter, K. & Lodato, G. 2016, *ARA&A*, 54, 271
 Kunitomo, M., Guillot, T., Ida, S., & Takeuchi, T. 2018, *A&A*, 618, A132
 Laughlin, G. & Adams, F. C. 1997, *ApJ*, 491, L51
 Maldonado, J., Micela, G., Baratella, M., et al. 2020, *A&A*, 644, A68
 Maldonado, J. & Villaver, E. 2016, *A&A*, 588, A98
 Maldonado, J., Villaver, E., & Eiroa, C. 2013, *A&A*, 554, A84
 Manara, C. F., Ansdell, M., Rosotti, G. P., et al. 2023, in *Astronomical Society of the Pacific Conference Series*, Vol. 534, *Protostars and Planets VII*, ed. S. Inutsuka, Y. Aikawa, T. Muto, K. Tomida, & M. Tamura, 539
 Meeus, G., Waters, L. B. F. M., Bouwman, J., et al. 2001, *A&A*, 365, 476
 Mendigutía, I., Lillo-Box, J., Vioque, M., et al. 2024, *A&A*, 686, L1
 Mendigutía, I., Mora, A., Montesinos, B., et al. 2012, *A&A*, 543, A59

- Mordasini, C., Alibert, Y., Benz, W., Klahr, H., & Henning, T. 2012, A&A, 541, A97
- Nayakshin, S. 2015, MNRAS, 448, L25
- Oh, S., Price-Whelan, A. M., Brewer, J. M., et al. 2018, ApJ, 854, 138
- Paxton, B., Bildsten, L., Dotter, A., et al. 2011, ApJS, 192, 3
- Paxton, B., Cantiello, M., Arras, P., et al. 2013, ApJS, 208, 4
- Paxton, B., Marchant, P., Schwab, J., et al. 2015, ApJS, 220, 15
- Paxton, B., Schwab, J., Bauer, E. B., et al. 2018, ApJS, 234, 34
- Paxton, B., Smolec, R., Schwab, J., et al. 2019, ApJS, 243, 10
- Peacock, J. A. 1983, MNRAS, 202, 615
- Perryman, M. 2018, The Exoplanet Handbook
- Pollack, J. B., Hubickyj, O., Bodenheimer, P., et al. 1996, Icarus, 124, 62
- Rauer, H., Catala, C., Aerts, C., et al. 2014, Experimental Astronomy, 38, 249
- Reffert, S., Bergmann, C., Quirrenbach, A., Trifonov, T., & Künstler, A. 2015, A&A, 574, A116
- Rice, W. K. M. & Armitage, P. J. 2003, ApJ, 598, L55
- Saffe, C., Alacoria, J., Miquelarena, P., et al. 2022, A&A, 668, A157
- Saffe, C., Miquelarena, P., Alacoria, J., et al. 2021, A&A, 647, A49
- Santos, N. C., Israelian, G., & Mayor, M. 2004, A&A, 415, 1153
- Schneider, J., Dedieu, C., Le Sidaner, P., Savalle, R., & Zolotukhin, I. 2011, A&A, 532, A79
- Scholz, F. W. & Stephens, M. A. 1987, Journal of the American Statistical Association, 82, 918
- Soares, B. M. T. B., Adibekyan, V., Mordasini, C., et al. 2025, A&A, 693, A47
- Sousa, S. G., Santos, N. C., Israelian, G., Mayor, M., & Udry, S. 2011, A&A, 533, A141
- Speedie, J., Dong, R., Hall, C., et al. 2024, Nature, 633, 58
- Stapper, L. M., Hogerheijde, M. R., van Dishoeck, E. F., & Mentel, R. 2022a, A&A, 658, A112
- Stapper, L. M., Hogerheijde, M. R., van Dishoeck, E. F., & Mentel, R. 2022b, A&A, 667, C1
- Udry, S. & Santos, N. C. 2007, ARA&A, 45, 397
- Villaver, E. & Livio, M. 2009, ApJ, 705, L81
- Villaver, E., Livio, M., Mustill, A. J., & Siess, L. 2014, ApJ, 794, 3
- Vioque, M., Oudmaijer, R. D., Wichittanakom, C., et al. 2022, ApJ, 930, 39
- Wichittanakom, C., Oudmaijer, R. D., Fairlamb, J. R., et al. 2020, MNRAS, 493, 234
- Wolthoff, V., Reffert, S., Quirrenbach, A., et al. 2022, A&A, 661, A63

Acknowledgements. J. M. acknowledges support from the Italian Ministero dell’Università e della Ricerca and the European Union - Next Generation EU through project PRIN 2022 PM4JLH “Know your little neighbours: characterising low-mass stars and planets in the Solar neighbourhood”. G. M. M. acknowledges support from the project AST22_00001_8 of the Junta de Andalucía and the Spanish Ministerio de Ciencia, Innovación y Universidades funded by the Next Generation EU and the Plan de Recuperación, Transformación y Resiliencia. I. M. ’s research is funded by grants PID2022-138366NA-I00, by the Spanish Ministry of Science and Innovation/State Agency of Research MCIN/AEI/10.13039/501100011033 and by the European Union, and by a Ramón y Cajal fellowship RyC2019-026992-I. E. V. , B. M. and J. L. G. M. acknowledge the funding by grant PID2021-127289-NB-I00 from MCIN/AEI/10.13039/501100011033/ and FEDER.

Appendix A: Online material

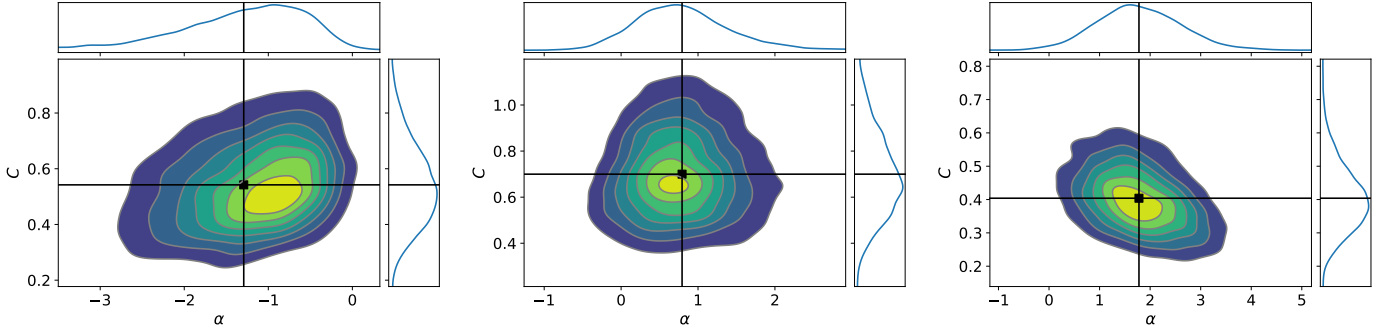


Fig. A.1. Marginal posterior probability distribution functions of the Bayesian fit to Eq. 2 for pre-MS stars (left), MS (middle), and giant stars (right). The vertical line indicates the mean of the distribution.

Table A.1. Stellar parameters of the pre-MS stars.

Star	Group	T_{eff} (K)	[Fe/H] (dex)	M_{\star} (M_{\odot})	Age (Myr)
HD 9672	I	9000 ± 125	0.20 ± 0.10	1.93 ± 0.03	11.0 ± 5.10
HD 31648	I	8000 ± 125	-0.25 ± 0.13	1.85 ± 0.03	7.7 ± 0.30
UX Ori	I	8500 ± 250	0.00 ± 0.10	1.91 ± 0.02	9.8 ± 0.10
HD 290380	I	6250 ± 125	0.00 ± 0.10	1.59 ± 0.06	9.3 ± 1.00
HD 287823	II	8375 ± 125	-0.50 ± 0.14	1.83 ± 0.04	10.6 ± 2.00
V346 Ori	II	7750 ± 250	0.00 ± 0.13	1.65 ± 0.04	16.2 ± 4.40
CO Ori	I	6500 ± 215	0.15 ± 0.10	2.30 ± 0.33	3.9 ± 1.60
HD 290500	II	9500 ± 500	0.00 ± 0.10	1.85 ± 0.03	< 19.9
HD 244314	I	8500 ± 250	0.00 ± 0.10	2.12 ± 0.06	7.0 ± 0.30
HD 244604	I	9000 ± 250	0.50 ± 0.10	2.16 ± 0.03	5.1 ± 0.10
RY Ori	I	6250 ± 194	0.00 ± 0.14	1.58 ± 0.17	9.4 ± 2.30
HD 245185	II	10000 ± 500	-0.50 ± 0.30	2.24 ± 0.03	7.1 ± 0.00
NV Ori	II	7000 ± 125	0.14 ± 0.10	2.09 ± 0.08	5.0 ± 0.50
HD 37258	I	9750 ± 500	0.35 ± 0.10	2.27 ± 0.06	5.9 ± 0.90
HD 290770	I	10500 ± 250	-1.00 ± 0.33	2.64 ± 0.09	4.0 ± 0.20
BF Ori	I	9000 ± 250	0.20 ± 0.13	1.85 ± 0.08	17.1 ± 1.40
HD 37357	I	9500 ± 250	0.50 ± 0.20	2.80 ± 0.20	3.0 ± 0.60
HD 290764	II	7875 ± 375	-0.15 ± 0.10	1.99 ± 0.04	6.1 ± 0.40
V599 Ori	II	8000 ± 250	-0.35 ± 0.10	2.15 ± 0.11	5.1 ± 0.70
V350 Ori	I	9000 ± 250	0.50 ± 0.10	< 1.91	< 15.0
HD 39014	I	8000 ± 125	0.20 ± 0.20	2.48 ± 0.07	3.5 ± 0.30
PDS 124	II	10250 ± 250	0.10 ± 0.15	2.38 ± 0.04	6.0 ± 0.40
LkHa 339	II	10500 ± 250	0.50 ± 0.12	2.52 ± 0.10	4.9 ± 0.30
HBC 217	II	6000 ± 125	-0.25 ± 0.10	1.75 ± 0.10	6.9 ± 1.30
HD 68695	II	9250 ± 250	-0.50 ± 0.10	2.08 ± 0.05	8.0 ± 0.80
GSC 8581-2002	II	9750 ± 250	0.00 ± 0.10	2.40 ± 0.05	5.1 ± 0.50
PDS 33	II	9750 ± 250	-0.50 ± 0.17	< 2.10	< 9.20
HD 97048	II	10500 ± 500	-0.50 ± 0.13	2.80 ± 0.03	3.9 ± 0.30
HD 100453	II	7250 ± 250	-0.10 ± 0.10	1.60 ± 0.05	19.3 ± 0.70
HD 132947	I	10250 ± 250	0.20 ± 0.10	2.77 ± 0.03	3.7 ± 0.40
HD 135344B	II	6375 ± 125	0.00 ± 0.13	1.46 ± 0.06	10.5 ± 0.70
HD 139614	II	7750 ± 250	-0.25 ± 0.10	1.60 ± 0.01	19.3 ± 0.30
HD 141569	I	9500 ± 250	-0.50 ± 0.38	2.12 ± 0.03	8.0 ± 0.00
HD 142666	I	7250 ± 250	0.00 ± 0.10	1.75 ± 0.02	8.7 ± 0.40
HD 142527	II	6500 ± 250	0.08 ± 0.13	2.20 ± 0.05	4.4 ± 0.40
HD 144432	I	7500 ± 250	0.15 ± 0.10	1.82 ± 0.02	8.0 ± 0.10
V718 Sco	I	7750 ± 250	0.00 ± 0.10	1.71 ± 0.03	9.0 ± 0.30
HD 149914	I	9500 ± 125	0.00 ± 0.14	3.07 ± 0.06	2.0 ± 0.00
HD 150193	I	9250 ± 250	0.20 ± 0.10	2.25 ± 0.04	6.0 ± 0.50
HD 163296	I	9000 ± 250	0.20 ± 0.10	1.91 ± 0.06	10.0 ± 5.80
HD 169142	II	7250 ± 125	-0.50 ± 0.33	1.55 ± 0.02	< 20
HD 179218	II	9500 ± 250	-0.50 ± 0.17	2.99 ± 0.03	2.3 ± 0.20
PX Vul	I	6500 ± 125	0.00 ± 0.10	2.59 ± 0.16	3.0 ± 0.40
HD 199603	I	7500 ± 125	0.00 ± 0.10	2.10 ± 0.05	5.2 ± 0.40

Table A.2. Stellar parameters of the Main-Sequence stars.

Star	Planet	T_{eff} (K)	[Fe/H] (dex)	M_{\star} (M_{\odot})	Age (Gyr)
WASP-33	y	7373 ± 164	0.13 ± 0.16	1.533 ± 0.067	0.527 ± 0.369
HD 23281		7761 ± 135	0.11 ± 0.10	1.613 ± 0.056	0.387 ± 0.244
HAT-P-70	y	8450 ± 195	-0.29 ± 0.15	1.648 ± 0.092	0.840 ± 0.338
beta Pic	y	8084 ± 130	-0.26 ± 0.14	1.551 ± 0.062	0.593 ± 0.332
V435 Car		7510 ± 165	-0.11 ± 0.09	1.546 ± 0.078	0.900 ± 0.463
HD 50445		7922 ± 117	-0.28 ± 0.16	1.560 ± 0.062	1.031 ± 0.281
HD 56537		8231 ± 122	-0.43 ± 0.16	1.810 ± 0.064	1.053 ± 0.090
KELT-19A	y	7500 ± 130	0.41 ± 0.17	1.656 ± 0.048	0.337 ± 0.210
KELT-17	y	7471 ± 210	0.51 ± 0.17	1.703 ± 0.042	0.333 ± 0.208
HAT-P-69	y	7750 ± 245	0.07 ± 0.15	1.722 ± 0.086	0.605 ± 0.358
MASCARA-4	y	7810 ± 165	-0.17 ± 0.12	1.618 ± 0.077	1.102 ± 0.290
HD 88955		8733 ± 154	-0.45 ± 0.13	1.778 ± 0.068	0.951 ± 0.129
HD 95086	y	7593 ± 122	-0.05 ± 0.16	1.511 ± 0.061	0.520 ± 0.345
HR 4502		9569 ± 253	-0.11 ± 0.10	2.058 ± 0.079	0.261 ± 0.125
HD 105850		9052 ± 167	-0.24 ± 0.13	1.883 ± 0.081	0.599 ± 0.173
WASP-167	y	6770 ± 210	0.03 ± 0.15	1.581 ± 0.058	1.504 ± 0.406
HD 115820		7610 ± 135	-0.02 ± 0.09	1.520 ± 0.061	0.503 ± 0.334
HD 129926		7101 ± 167	0.38 ± 0.12	1.588 ± 0.067	0.512 ± 0.371
WASP-189	y	7946 ± 136	0.05 ± 0.13	1.866 ± 0.073	0.814 ± 0.177
HD 146624		9489 ± 184	0.01 ± 0.11	2.006 ± 0.053	0.208 ± 0.088
HD 153053		7916 ± 129	-0.22 ± 0.15	1.619 ± 0.068	1.099 ± 0.238
HD 159492		8076 ± 128	-0.02 ± 0.11	1.707 ± 0.069	0.468 ± 0.259
Vega		9505 ± 188	-0.72 ± 0.08	2.037 ± 0.075	0.721 ± 0.071
KELT-20	y	8652 ± 160	-0.30 ± 0.15	1.703 ± 0.078	0.709 ± 0.258
HD 188228		10262 ± 172	0.02 ± 0.08	2.201 ± 0.037	0.144 ± 0.039
KELT-9	y	9329 ± 118	-0.08 ± 0.14	2.215 ± 0.070	0.482 ± 0.078
MASCARA-1	y	7687 ± 238	-0.10 ± 0.13	1.704 ± 0.074	0.988 ± 0.287
Fomalhaut		8745 ± 195	0.11 ± 0.15	1.949 ± 0.071	0.295 ± 0.154

Table A.3. Stellar parameters of the red giant stars.

Star	Planet	T_{eff} (K)	[Fe/H] (dex)	M_{\star} (M_{\odot})	Age (Gyr)
HIP 671	y	4829 ± 10	-0.13 ± 0.02	1.68 ± 0.05	1.97 ± 0.17
HIP 729		4811 ± 23	0.04 ± 0.04	1.81 ± 0.08	1.77 ± 0.19
HIP 873		4849 ± 15	0.03 ± 0.02	1.78 ± 0.05	1.72 ± 0.14
HIP 5364	y	4594 ± 25	0.10 ± 0.04	1.63 ± 0.17	2.45 ± 0.82
HIP 6999		4961 ± 20	0.07 ± 0.03	2.43 ± 0.08	0.76 ± 0.09
HIP 7097		4936 ± 40	-0.09 ± 0.06	3.62 ± 0.14	0.24 ± 0.03
HIP 7607		4396 ± 38	0.11 ± 0.07	1.85 ± 0.20	1.78 ± 0.49
HIP 7719		5097 ± 20	-0.12 ± 0.02	2.32 ± 0.10	0.77 ± 0.11
HIP 8928	y	4917 ± 10	-0.25 ± 0.02	1.65 ± 0.08	1.97 ± 0.24
HIP 9222		4803 ± 10	-0.15 ± 0.02	1.52 ± 0.04	2.51 ± 0.20
HIP 11791	y	4884 ± 15	-0.01 ± 0.02	1.94 ± 0.09	1.54 ± 0.19
HIP 12247	y	4864 ± 23	-0.03 ± 0.03	1.83 ± 0.09	1.68 ± 0.18
HIP 13531		5025 ± 25	-0.20 ± 0.03	2.91 ± 0.08	0.43 ± 0.04
HIP 19038		4808 ± 28	0.09 ± 0.04	2.24 ± 0.12	1.09 ± 0.21
HIP 20889	y	4911 ± 25	0.15 ± 0.04	2.63 ± 0.07	0.63 ± 0.07
HIP 31674	y	4884 ± 10	-0.06 ± 0.02	1.71 ± 0.03	1.83 ± 0.09
HIP 36616	y	4669 ± 20	0.13 ± 0.04	1.98 ± 0.19	1.48 ± 0.46
HIP 37826	y	4887 ± 18	0.09 ± 0.03	2.03 ± 0.07	1.31 ± 0.17
HIP 42528		5128 ± 20	0.01 ± 0.03	1.76 ± 0.05	1.75 ± 0.13
HIP 57820	y	4978 ± 30	0.14 ± 0.04	1.56 ± 0.09	2.68 ± 0.47
HIP 59646		5132 ± 23	0.10 ± 0.03	1.52 ± 0.03	2.87 ± 0.14
HIP 59847		4872 ± 20	-0.20 ± 0.03	1.61 ± 0.12	2.16 ± 0.44
HIP 59856		4581 ± 28	-0.12 ± 0.05	1.85 ± 0.14	1.57 ± 0.32
HIP 61740	y	4605 ± 40	0.35 ± 0.06	2.94 ± 0.10	0.46 ± 0.07
HIP 69612		4809 ± 23	-0.08 ± 0.03	1.61 ± 0.11	2.29 ± 0.44
HIP 70038		5071 ± 23	-0.04 ± 0.03	2.04 ± 0.07	1.11 ± 0.10
HIP 74793	y	4260 ± 33	0.00 ± 0.06	1.69 ± 0.18	2.08 ± 0.65
HIP 76311	y	4601 ± 28	0.34 ± 0.05	2.16 ± 0.18	1.19 ± 0.33
HIP 80816		5000 ± 20	-0.10 ± 0.03	2.89 ± 0.07	0.45 ± 0.04
HIP 88765		4998 ± 15	-0.01 ± 0.03	2.68 ± 0.07	0.56 ± 0.06
HIP 88836		4647 ± 33	0.21 ± 0.06	1.52 ± 0.10	2.96 ± 0.56
HIP 89047	y	4983 ± 10	0.03 ± 0.02	1.53 ± 0.02	2.69 ± 0.09
HIP 89826		4639 ± 28	0.13 ± 0.05	2.62 ± 0.18	0.66 ± 0.17
HIP 89918		5061 ± 18	-0.09 ± 0.02	2.45 ± 0.07	0.69 ± 0.08
HIP 91852	y	4775 ± 30	-0.12 ± 0.04	1.83 ± 0.24	1.62 ± 0.60
HIP 95124	y	4998 ± 15	0.20 ± 0.03	1.71 ± 0.07	2.07 ± 0.24
HIP 95822		4819 ± 25	0.07 ± 0.03	1.92 ± 0.14	1.61 ± 0.29
HIP 96016		4997 ± 13	-0.13 ± 0.02	1.57 ± 0.04	2.27 ± 0.15
HIP 98920		4775 ± 28	0.09 ± 0.04	1.60 ± 0.08	2.43 ± 0.33
HIP 99841		5024 ± 15	-0.11 ± 0.02	2.16 ± 0.09	1.00 ± 0.15
HIP 99913		4805 ± 15	0.07 ± 0.03	1.87 ± 0.05	1.62 ± 0.14
HIP 100541		4932 ± 20	-0.06 ± 0.03	1.95 ± 0.10	1.44 ± 0.23
HIP 101936		4796 ± 33	0.07 ± 0.05	1.83 ± 0.13	1.76 ± 0.31
HIP 102532		4801 ± 18	0.13 ± 0.03	1.94 ± 0.05	1.48 ± 0.12
HIP 103004		5261 ± 15	-0.05 ± 0.02	2.40 ± 0.05	0.70 ± 0.04
HIP 103519		4993 ± 20	0.12 ± 0.03	2.33 ± 0.05	0.80 ± 0.04
HIP 103527	y	5106 ± 30	0.07 ± 0.04	2.28 ± 0.04	0.84 ± 0.03
HIP 104202	y	5067 ± 20	-0.11 ± 0.03	1.53 ± 0.05	2.50 ± 0.20
HIP 105411		4809 ± 25	-0.10 ± 0.03	1.77 ± 0.15	1.65 ± 0.43
HIP 106093		4953 ± 15	0.06 ± 0.03	2.02 ± 0.07	1.26 ± 0.16
HIP 107251	y	4953 ± 45	0.22 ± 0.06	1.74 ± 0.21	1.97 ± 0.70
HIP 108513	y	4889 ± 15	0.17 ± 0.03	1.56 ± 0.04	2.72 ± 0.16
HIP 109577	y	4993 ± 15	0.02 ± 0.02	1.63 ± 0.03	2.24 ± 0.12
HIP 111944		4352 ± 25	-0.19 ± 0.05	1.66 ± 0.16	1.97 ± 0.57
HIP 112158		4986 ± 20	-0.21 ± 0.03	3.30 ± 0.09	0.30 ± 0.03
HIP 112242		5035 ± 20	0.10 ± 0.03	2.59 ± 0.04	0.59 ± 0.02
HIP 115830		4756 ± 25	0.08 ± 0.04	1.83 ± 0.05	1.72 ± 0.13
HIP 115919		5034 ± 15	0.05 ± 0.03	2.39 ± 0.06	0.74 ± 0.05
HIP 117375		5010 ± 25	-0.05 ± 0.03	2.32 ± 0.09	0.85 ± 0.12